

Deformed crystals and torsional oscillations of neutron star crust

A. A. Kozhberov^{*}, D. G. Yakovlev

Ioffe Institute, Politekhnicheskaya 26, St Petersburg 194021, Russia

September 25, 2020

ABSTRACT

We study breaking stress of deformed Coulomb crystals in a neutron star crust, taking into account electron plasma screening of ion-ion interaction; calculated breaking stress is fitted as a function of electron screening parameter. We apply the results for analyzing torsional oscillation modes in the crust of a non-magnetic star. We present exact analytic expression for the fundamental frequencies of such oscillations and show that the frequencies of all torsional oscillations are insensitive to the presence of the outer neutron star crust. The results can be useful in theoretical modeling of processes involving deformed Coulomb crystals in the crust of neutron stars, such as magnetic field evolution, torsional crustal or magneto-elastic quasi-periodic oscillations of flaring soft gamma-ray repeaters, pulsar glitches. The applicability of the results to soft gamma-ray repeaters is discussed.

Key words: stars: neutron – dense matter – stars: oscillations (including pulsations)

1 INTRODUCTION

Neutron stars are thought to have a bulky and massive liquid core of superdense matter (e.g., Shapiro & Teukolsky 1983). The core is surrounded by a thin and light envelope (with thickness ~ 1 km and with mass of $\sim 0.01 M_{\odot}$) which is often called the crust; its matter contains ions (atomic nuclei), electrons and possibly free neutrons. The ions constitute the Coulomb plasma (e.g. Haensel et al. 2007) which is typically in crystalline state but may be liquid or gaseous especially in the surface layers of warm stars.

The crust is known to be divided into the outer crust ($\rho \leq \rho_{\text{drip}} = 4.3 \times 10^{11} \text{ g cm}^{-3}$) and the deeper inner crust. The outer crust consists predominantly of the ions and electrons. At $\rho \gtrsim 10^6 \text{ g cm}^{-3}$ (about 10 m under the neutron star surface) the ions become fully ionized and the electrons become strongly degenerate and relativistic. In the inner crust, free neutrons appear in addition to the ions and electrons; they are dripped off the nuclei and further complicate nuclear physics of the crust. The free neutrons are typically degenerate and superfluid.

Crystalline ions in the crust can be described by the Coulomb crystal model. This model is also used in the physics of white dwarfs as well as in the physics of dusty plasmas, available in space and laboratory, with numerous applications in science and technology (see, e.g., Vaulina et al. 2010 and references therein). Here we primarily consider

neutron star matter. To study Coulomb lattice, one commonly employs a model of ion-ion interaction screened by polarization of plasma electrons (as detailed in Section 2.1). The electron screening is relatively weak through the crust bulk, at $\rho \gtrsim 10^6 \text{ g cm}^{-3}$, although one usually takes it into account (e.g., Chugunov & Horowitz 2010). At smaller densities, the electron plasma screening can be stronger but the electron screening model can be more complicated because of partial ionization of ions.

When neutron stars evolve, their crust undergoes various deformations (e.g., Owen 2005; Chamel & Haensel 2008; Baiko & Kozhberov 2017; Fattoyev et al. 2018; Gabler et al. 2018; Baiko & Chugunov 2018). For magnetars, these deformations are primarily associated with the magnetic field (e.g., Beloborodov & Levin 2014; Lander 2016; Li et al. 2016); for pulsars they are thought to be connected with glitches (e.g., Piekarewicz et al. 2014). Investigations of deformed lattices are important for understanding different processes in neutron star interiors.

In Section 2 we consider properties of deformed Coulomb crystals with the focus on the effect of electron plasma screening of the ion-ion interaction on the breaking stress. Stronger screening simplifies the breaking; one should study the strength of this effect for modeling various phenomena associated with deformations of Coulomb crystals. We calculate the breaking stress of mono-crystals under some specific deformations and approximate the results by an accurate analytic function of the electron screening parameter. We outline further breaking stress of poly-

^{*} E-mail: kozhberov@gmail.com

crystals (isotropic solids); this model is common in neutron star physics.

In Sections 3 and 4 we investigate torsional oscillations of neutron stars which are determined by elastic properties of Coulomb crystals. Torsional oscillations are widely used to explain quasi-periodic oscillations (QPOs) in the spectra of soft gamma-ray repeaters (SGRs); see e.g. [Watts & Strohmayer \(2006\)](#); [Huppenkothen et al. \(2014a,b\)](#). There are many theoretical investigations of torsional (crustal elastic) and magneto-elastic oscillations of neutron stars aimed at explaining observed QPO frequencies; e.g., [Gabler et al. \(2016, 2018\)](#) and references therein.

We will study torsional oscillations of non-rotating and non-magnetic stars. In spite of many publications, not all their properties have been investigated in detail. Our primary interest will be in analytic analysis of oscillation spectrum, energy, breaking conditions and special behavior of outer crystallized layers in these oscillations. We discuss and conclude in Section 5.

2 DEFORMED COULOMB CRYSTALS IN NEUTRON STARS

2.1 Main parameters

In this section we summarize the data on deformed Coulomb crystals of atomic nuclei in a neutron star crust paying special attention on the maximum (breaking) stress. We will consider widely used models of the crust which contains ions (spherical atomic nuclei) of one type in a given matter element. Type and properties of atomic nuclei change with the density ρ (e.g., [Haensel et al. 2007](#)), from ordinary nuclei (such as ^4He , ^{12}C , ^{56}Fe) near the surface to very neutron rich nuclei at the crust-core interface (at $\rho_{cc} \approx 1.5 \times 10^{14} \text{ g cm}^{-3}$) which would be highly unstable in laboratory. Variation of atomic nucleus parameters with depth is a complicated phenomenon governed by nuclear physics and by pre-history of crustal matter (accretion, cooling, nuclear burning, beta-processes).

In spite of the complexity of nuclear physics, the description of Coulomb crystals of atomic nuclei is based on a few simple parameters (e.g., [Haensel et al. 2007](#)),

$$\Gamma = \frac{Z^2 e^2}{a_i k_B T}, \quad a_i = \left(\frac{3}{4\pi n_i} \right)^{1/3}, \quad (1)$$

where Γ is the Coulomb coupling parameter, $n_i = N_i/V$ is the number density of the ions, Z is the charge number of one ion, N_i is the number of ions (in a volume V), a_i is the ion-sphere (Wigner-Seitz) radius, T the temperature, e the elementary charge, and k_B the Boltzmann constant. A classical system of the ions solidifies at $\Gamma \geq \Gamma_m \approx 175$, i.e. at $T \leq T_m \approx Z^2 e^2 / (k_B a_i \Gamma_m)$.

While simulating Coulomb plasmas of ions one often uses the model of exponentially screened Coulomb interaction for a pair of ions,

$$U(r) = \frac{Z^2 e^2}{r} \exp(-\kappa r), \quad (2)$$

where r is a distance between the ions, and κ is an inverse electron plasma screening length. In the very outer neutron star layers, where the electrons are non-degenerate, κ is equal to the inverse electron Debye screening length. In

the deeper layers of strongly degenerate electrons, it is the Thomas-Fermi electron wavenumber,

$$\kappa_{\text{TF}} \equiv \sqrt{4\pi e^2 \frac{\partial n_e}{\partial \mu_e}} = \frac{p_F}{\hbar} \left(\frac{4e^2}{\pi v_F} \right)^{1/2}, \quad (3)$$

where $n_e = Zn_i$ is the number density of electrons, μ_e is the electron chemical potential, p_F the electron Fermi momentum, and v_F is the electron Fermi velocity.

We will be mainly interested in these deeper layers. The electron screening of the inter-ion potential (2) can be characterized by the dimensionless screening parameter $s \equiv \kappa a_i$ that is typically small but generally non-negligible. The case of $s = 0$ corresponds to the absence of plasma screening. For the screening by degenerate electrons, from equation (3) we have

$$s = \kappa_{\text{TF}} a_i = 0.1850 Z^{1/3} \frac{c}{v_F}, \quad (4)$$

where c is the velocity of light. Through the bulk of the crust, for any composition of the crustal matter (e.g., [Haensel et al. 2007](#)) one has $s \lesssim 0.7$. Higher s may be realized in a narrow layer near the surface, at $\rho \lesssim 10^6 \text{ g cm}^{-3}$. However, the applicability of the screened Coulomb potential given by equation (2) in this layer requires further study because of the effects of partial ionization.

2.2 Breaking stress of Coulomb crystals

Let us outline theoretical data on the breaking stress σ_{max} of Coulomb crystals, paying particular attention on its dependence on s .

Most of the previous studies of stressed Coulomb crystals have focused on the shear modulus μ of these crystals (e.g., [Ogata & Ichimaru 1990](#); [Strohmayer et al. 1991](#); [Horowitz & Hughto 2008](#); [Horowitz & Kadau 2009](#); [Hughto 2012](#); [Chugunov & Horowitz 2012](#)), paying less attention to their stability. Analytically, it has been done by [Baiko & Kozhberov \(2017\)](#); [Baiko & Chugunov \(2018\)](#) for the bcc lattice with the uniform electron background. Deformations of lattices with $s > 0$ have been investigated by [Chugunov & Horowitz \(2010\)](#); [Hoffman & Heyl \(2012\)](#) via molecular dynamic (MD) simulations for a restricted number of s values; these results will be discussed further.

For obtaining σ_{max} we need the potential energy of a Coulomb crystal. Let a distance between two ions i and j be $r_{ij} = |\mathbf{R}_i - \mathbf{R}_j + \mathbf{u}_i - \mathbf{u}_j|$, where \mathbf{R}_i is the equilibrium position of the i th ion, and \mathbf{u}_i is its displacement. At $\Gamma \gg \Gamma_m$, motions of crystalline ions can be considered as small oscillations around their equilibrium positions. Then their potential energy can be expanded in powers of \mathbf{u}_i ,

$$U_i \approx U_M + \frac{1}{2} \sum_{i,j=1}^{N_i} u_i^\alpha u_j^\beta \frac{\partial^2 U_i}{\partial u_i^\alpha \partial u_j^\beta} \Big|_{u_i^\alpha, u_j^\beta=0}, \quad (5)$$

where Greek indices enumerate Cartesian vector components, and summation over repeated indices is assumed; U_M is the electrostatic (Madelung) energy of the lattice.

For any lattice with one ion in the elementary cell at $s \geq 0$, the electrostatic energy can be written as (e.g., [Baiko](#)

2002)

$$U_M = N_i \frac{Z^2 e^2}{a_i} \zeta, \quad (6)$$

$$\begin{aligned} \frac{\zeta}{a_i} &= \sum_{l \neq 0} \frac{E_- + E_+}{4R_l} - \frac{\kappa}{2} \operatorname{erf} \left(\frac{\kappa^2}{2A^2} \right) - \frac{A}{\sqrt{\pi}} e^{-\frac{\kappa^2}{4A^2}} \\ &+ \sum_m \frac{2\pi n_i}{G_m^2 + \kappa^2} e^{-\frac{G_m^2 + \kappa^2}{4A^2}} - \frac{2\pi n_i}{\kappa^2}, \end{aligned} \quad (7)$$

where $E_{\pm} = e^{\pm \kappa R_l} \operatorname{erfc}(AR_l \pm \kappa/(2A))$, \mathbf{R}_l is a direct lattice vector, \mathbf{G}_m is a reciprocal lattice vector, $\operatorname{erf}(x)$ is the error function, $\operatorname{erfc}(x) \equiv 1 - \operatorname{erf}(x)$, and A is an arbitrary constant; $A \approx 2/a_i$ is most suitable because it gives good numerical convergence of the sums.

We assume that the ions form a body-centered cubic (bcc) lattice because at $s = 0$. This lattice possesses the lowest electrostatic energy; its Madelung constant $\zeta = -0.895929255682$ (e.g., [Chamel & Fantina 2016](#)). The dependence of ζ on s is naturally the same for degenerate and non-degenerate electron background as long as the ion-ion interaction is described by equation (2). For degenerate relativistic electrons in the envelopes of neutron stars, according to equation (4), we have $s \lesssim 0.7$. For non-degenerate (or degenerate but non-relativistic) electrons this criterion can be formally less strict ([Hamaguchi & Farouki 1994](#)), but it is limited by partial ionization of ions and associated screening of the inter-ion interaction by bound electrons.

Here, we present the first semi-analytical study of stability of a deformed bcc Coulomb crystal with $s > 0$. Let us introduce a Cartesian coordinate system with the main lattice cube edges of the bcc lattice oriented in such a way that the direction to the nearest neighbor is given by vector $0.5a_1(1, 1, 1)$, a_1 being the lattice constant. Following [Chugunov & Horowitz \(2010\)](#), we consider such deformation of this lattice, which translates the vector $a_1(n_1, n_2, n_3)$ as

$$a_1(n_1, n_2, n_3) \rightarrow a_1 \left(n_1 + \frac{\epsilon}{2} n_2, n_2 + \frac{\epsilon}{2} n_1, \frac{n_3}{1 - \epsilon^2/4} \right), \quad (8)$$

where ϵ is a small deformation parameter, while n_1, n_2 , and n_3 are arbitrary integers.

With increasing ϵ the crystal becomes more strained and stressed. It breaks at some critical $\epsilon = \epsilon_{\max}$ which depends on s . The effective stress at any ϵ is calculated as

$$\sigma(s, \epsilon) = \frac{\partial \mathcal{E}}{\partial \epsilon} = n_i \frac{Z^2 e^2}{a_i} \frac{\partial \zeta}{\partial \epsilon}, \quad (9)$$

where we take the Madelung energy U_M as an internal energy at zero temperature and neglect the energy of ion vibrations, so that the internal energy density of the ions is $\mathcal{E} = U_M/V$. The breaking stress is then given by $\sigma_{\max}(s) \equiv \sigma(s, \epsilon_{\max})$ (e.g., [Chugunov & Horowitz 2010](#)). For a crystal with the uniform electron background ($s = 0$), one has $\epsilon_{\max} = 0.1109$.

MD studies determine ϵ_{\max} and σ_{\max} through direct simulations of crystal evolution under increasing ϵ .

In semi-analytical studies, the lattice at low temperatures can be treated as unstable if one or more of the squared frequencies of phonon modes become negative at some phonon wave vector. In other words, in a stable crystal the second-order term in equation (5) should be a positive definite quadratic form. Increasing the plasma screening s

Table 1. Breaking strain ϵ_{\max} and stress σ_{\max} versus s at $T = 0$ for transformation (8) of the bcc lattice

s	ϵ_{\max}	$\tilde{\sigma}_{\max}^{(a)}$	s	ϵ_{\max}	$\tilde{\sigma}_{\max}$
0.0	0.1109	0.02007	1.3	0.0998	0.01651
0.4	0.1099	0.01972	1.42	0.0979	0.01591
0.5714	0.1090	0.01938	1.53	0.0957	0.01529
0.71	0.1079	0.01901	1.62	0.0938	0.01477
0.87	0.1059	0.01841	1.73	0.0918	0.01417
1.04	0.1038	0.01773	1.81	0.0898	0.01366
1.19	0.1018	0.01708			

^{a)} $\tilde{\sigma}_{\max} = \sigma_{\max}/(n_i Z^2 e^2/a_i)$

makes the crystals less stable. For the bcc lattice, there exist a critical value $s_{\max} = 4.76$ which completely destroys crystalline state. It was calculated by [Robbins et al. \(1988\)](#) in MD simulations of the dusty plasma crystals; it was independently proven by [Kozhberov \(2018\)](#). It is not clear if this effect can be realized in the neutron stars because the applicability of equation (2) at so high s in neutron star matter is questionable, but the effect may take place in dusty plasmas (see Section 1).

For a given s , we have determined ϵ_{\max} as the critical strain, at which some phonon frequencies become complex numbers, and obtained then the breaking stress σ_{\max} from equation (9) at this ϵ_{\max} . In Table 1 we list ϵ_{\max} and σ_{\max} for a number of s values (with $s \leq 1.81$). Naturally, increasing the electron screening reduces ϵ_{\max} and σ_{\max} .

Note that the values of σ_{\max} from Table 1 can be accurately approximated as

$$\sigma_{\max}(s) = \sigma_{\max}(0) \frac{\sqrt{1 + 1.451 s^2}}{1 + 0.755 s^2}. \quad (10)$$

The root-mean squared relative error of this fit is 0.7 per cent, and the maximum error of 1.5 per cent occurs at $s = 1.81$.

Let us stress that we have calculated the phonon spectrum in the linear harmonic-lattice approximation. Such phonon frequencies are independent of temperature, and the approach is well justified for temperatures T , which are sufficiently lower than the melting temperature T_m . If T is close to T_m , the linear theory may become inaccurate because of anharmonic effects. Therefore, we warn the reader that our results (Table 1) can be inaccurate near the melting point.

Now we can compare our results with MD simulations performed by [Chugunov & Horowitz \(2010\)](#) at the one value of $s = 4/7 \approx 0.5714$. They approximated their results by

$$\sigma_{\max}^{\text{MD}}(4/7) = n_i \frac{Z^2 e^2}{a_i} \left(0.0195 - \frac{1.27}{\Gamma - 71} \right). \quad (11)$$

Then at small T their $\sigma_{\max}^{\text{MD}} = 0.0195 n_i Z^2 e^2/a_i$ deviates from our value (line 3 in our Table 1) only by a fraction of per cent. This good agreement supports practical equivalence of two criteria of stability — the MD one and the one based on complex-valued phonon modes. Note that [Chugunov & Horowitz \(2010\)](#) give the typical breaking strain $\epsilon_{\max} \approx 0.13$, which approximately agrees with our calculations. A slight difference can be explained by the fact that the part of the first Brillouin zone, where the complex-

Table 2. The same as in Table 1 but for the lattice transformation (12)

s	ϵ_{\max}	$\tilde{\sigma}_{\max}$
0	0.1051	0.01928
0.5	0.1036	0.01874
1	0.0990	0.01719

valued frequencies appear, is small and noticeably increases with ϵ (see Baiko & Kozhberov 2017).

We have also considered two other shear deformations of bcc lattice. The first one is

$$a_1(n_1, n_2, n_3) \rightarrow a_1(n_1 + n_3\epsilon, n_2, n_3), \quad (12)$$

where ϵ is again the deformation parameter. We have calculated the breaking stress σ_{\max} in the same way as in Table 1. The results are presented in Table 2 for $s=0, 0.5$ and 1. They are accurately fitted by the same equation (10), which fits the data of Table 1. Note that equation (10) is not supposed to be highly accurate for all shear deformations.

The next shear deformation is a compression ($\epsilon < 0$) neglecting the electron screening ($s = 0$), at which

$$a_1(n_1, n_2, n_3) \rightarrow a_1\left((1 + \epsilon)n_1, \frac{n_2}{\sqrt{1 + \epsilon}}, \frac{n_3}{\sqrt{1 + \epsilon}}\right). \quad (13)$$

According to Baiko & Chugunov (2018) at $\epsilon < 0$ it gives one of the lowest strains, $|\epsilon_{\max}| = 0.0435$. For this strain we have calculated $\partial\zeta/\partial\epsilon = 0.00542$, which yields $\sigma_{\max} = 0.00542 n_i Z^2 e^2 / a_i$ from equation (9). This demonstrates once again the well known fact that σ_{\max} and μ in a Coulomb crystal noticeably depend on deformation type (e.g. Baiko & Kozhberov 2017; Kozhberov 2018; Baiko & Chugunov 2018 and references therein). Note that the reported value of σ_{\max} is close to the value of $\mu \epsilon_{\max} \approx 0.0052 n_i Z^2 e^2 / a_i$, where μ is given by equation (14) presented below.

For practical applications in a neutron star crust we will consider the model of isotropic solid in which (Ogata & Ichimaru 1990)

$$\mu = 0.1194 n_i \frac{Z^2 e^2}{a_i}, \quad (14)$$

and take the maximum strength in the form

$$\sigma_{\max} \approx 0.02 n_i \frac{Z^2 e^2}{a_i}. \quad (15)$$

We have not found any deformation in a bcc mono-crystal, which gives significantly larger σ_{\max} . This value agrees with results of Hoffman & Heyl (2012); in all their simulations σ_{\max} has not been larger.

Please bear in mind that we have mainly discussed simulations in mono-crystals, whereas formation of polycrystals (particularly isotropic solids) in neutron star crust seems more likely. According to previous studies (Horowitz & Kadau 2009; Hoffman & Heyl 2012; Baiko & Chugunov 2018), equation (15) can be a reasonable estimate for polycrystals but numerical factor is uncertain, with typical values ranged around 0.01 (it can be about twice smaller or larger). Therefore, our analysis of breaking conditions in neutron star crust in the next sections should be regarded as qualitative.

3 TORSIONAL OSCILLATIONS OF NEUTRON STAR CRUST

3.1 Preliminaries

Let us apply the results of Section 2 to analyze torsional oscillations of neutron star crust. We will consider the simplest model of a non-rotating and non-magnetic neutron star with crystalline crust and liquid core. We will treat crustal matter as a poly-crystal (isotropic solid) based on the Coulomb lattice of spherical atomic nuclei of one type at any given density ρ . The density can range from the density of solidified (e.g. iron) matter in the surface layers to about one half of the saturation density of nuclear matter ($1.5 \times 10^{14} \text{ g cm}^{-3}$) at the crust-core interface (e.g., Haensel et al. 2007).

We will follow the theory of torsional oscillations developed in a very detailed paper by Schumaker & Thorne (1983). The authors have studied torsional oscillations taking into account associated space-time oscillations and emission of gravitational waves. Since these effects of General Relativity are tiny, we restrict ourselves by the relativistic Cowling approximation, in which case space-time is not perturbed and gravitational wave emission is neglected. This approximation is well justified and greatly simplifies theoretical consideration of the torsional oscillations.

3.2 General equations

Let us summarize the equations of Schumaker & Thorne (1983) neglecting space-time perturbations. The metric inside and outside of a spherically symmetric non-perturbed star is taken in the standard form

$$ds^2 = -e^{2\Phi} dt^2 + e^{2\Lambda} dr^2 + r^2(d\theta^2 + \sin^2\theta d\phi^2), \quad (16)$$

where t is Schwarzschild time (for a distant observer), r is a radial coordinate (circumferential radius), θ and ϕ are ordinary spherical angles, while Λ and Φ are two metric functions of r . At any r one has

$$\exp \Lambda(r) = \frac{1}{\sqrt{1 - 2Gm(r)/rc^2}}, \quad (17)$$

where $m(r)$ is the gravitational mass enclosed within a sphere of radius r and G is the gravitational constant.

Let $r = R$ be the radius of the star at which the pressure of the matter, $P(R) = 0$. Then $M = m(R)$ is the gravitational mass of the star. The functions $m(r)$, $P(r)$ and $\Phi(r)$ within the star are obtained from the standard equations of hydrostatic equilibrium [equations (5) in Schumaker & Thorne 1983], supplemented by the equation of state of stellar matter, which relates the pressure P with the energy density ρc^2 .

Note the relation [equation (5h) in Schumaker & Thorne 1983]

$$\Phi' + \Lambda' = 4\pi Gc^{-1}(\rho + P/c^2)\exp(2\Lambda), \quad (18)$$

where prime denotes differentiation with respect to r .

Outside the star ($r > R$) one has

$$\exp \Phi = \exp(-\Lambda) = \sqrt{1 - r_g/r}, \quad (19)$$

with $r_g = 2GM/c^2$ being the Schwarzschild radius.

3.3 Torsional oscillations

Torsional oscillations consist of shear motions of crystallized matter in the neutron star crust along spherical surfaces. In the adopted approximation, they are not accompanied by oscillations of density and pressure. The oscillations are weak and studied by linearizing the equations of shear motion. Then one comes (Schumaker & Thorne 1983) to a set of independent eigenmodes characterized by traditional spherical harmonics. Each mode can be specified by multipolarity $\ell = 2, 3, \dots$, azimuthal number ($-\ell \leq m_\ell \leq \ell$), as well as by the number of radial nodes $n = 0, 1, \dots$. The eigenfrequencies $\omega = \omega_{\ell n}$ are naturally degenerate in m_ℓ . In order to find the oscillation spectrum, it is sufficient to set $m_\ell = 0$. Then, among the three spacial coordinates (r, θ and ϕ) of a crystalline matter element, only the angle ϕ varies. A small proper spacial displacement of the matter element can be written as

$$dl = r Y(r) \exp(i\omega t) b_\ell(\theta), \quad b_\ell(\theta) = \frac{\partial}{\partial \theta} P_\ell(\cos \theta), \quad (20)$$

where $P_\ell(\cos \theta)$ is a Legendre polynomial. The dimensionless function $Y(r)$ is the radial part of the angular oscillation amplitude (to be calculated); it is real for our problem. A complex oscillating exponent $\exp(i\omega t)$ has to be understood in a standard way (as a real part). The function $b(\theta)$ describes the θ -dependence of the oscillation amplitude. For instance, $b_2(\theta) = 3 \cos \theta \sin \theta$ and $b_3(\theta) = 1.5(5 \cos^2 \theta - 1) \sin \theta$. At any ℓ the vibrational motion vanishes along at the ‘vibrational’ axis z [since one always has $b(\theta) \propto \sin \theta$]. If $\ell = 2$, the vibrational motion is absent also at the stellar equator; then crystal elements are shifting in opposite directions in the upper and lower hemispheres of the star. At $\ell = 3$ vibrations disappear along conical surfaces with $\cos^2 \theta = 1/5$, which separate the oscillating crust into three zones. Recall that we are discussing the oscillation modes with $m_\ell = 0$. Consideration of the modes with $m_\ell \neq 0$ is similar and standard (using spherical harmonics).

The equation for $Y(r)$ can be written as

$$Y'' + \left(\frac{4}{r} + \Phi' - \Lambda' + \frac{\mu'}{\mu} \right) Y' + \left[\frac{\rho + P/c^2}{\mu} \omega^2 e^{-2\Phi} - \frac{(\ell+2)(\ell-1)}{r^2} \right] e^{2\Lambda} Y = 0. \quad (21)$$

It follows from equation (19b) of Schumaker & Thorne (1983) and equation (18) and presented in many publications (e.g., Sotani et al. 2012). In order to determine the pulsation frequency, it has to be solved with the boundary conditions $Y'(r_1) = 0$ and $Y'(r_2) = 0$ at both (inner and outer) boundaries $r_{1,2}$ of the crystalline matter.

Note that the quantity

$$v_s(r) = \sqrt{\frac{\mu(r)}{\rho + P(r)/c^2}}, \quad (22)$$

in the square brackets of equation (21) is a local velocity of the radial shear wave as measured by a local observer.

3.4 Formal relations

Let us present some useful formal relations derived by Schumaker & Thorne (1983).

First of all, in the absence of dissipation, the vibrational

energy of any mode, as measured by a distant observer, is [equation (62a) in Schumaker & Thorne 1983]

$$E_{\text{vib}} = \frac{\pi \ell(\ell+1)}{2\ell+1} \int_{r_1}^{r_2} dr \left[\omega^2 (\rho + P/c^2) e^{\Lambda-\Phi} |Y|^2 + \mu r^4 e^{\Phi-\Lambda} |Y'|^2 + \mu(\ell+2)(\ell-1) r^2 e^{\Phi+\Lambda} |Y|^2 \right]. \quad (23)$$

Then from equations (58a–58c) in the relativistic Cowling approximation we obtain

$$\omega^2 = B/A, \quad (24)$$

$$A = \int_{r_1}^{r_2} dr (\rho + P/c^2) e^{\Lambda-\Phi} |Y|^2, \quad (25)$$

$$B = \int_{r_1}^{r_2} dr \left[\mu r^4 e^{\Phi-\Lambda} |Y'|^2 + \mu(\ell+2)(\ell-1) r^2 e^{\Phi+\Lambda} |Y|^2 \right]. \quad (26)$$

Clearly, A and B determine the vibrational energy E_{vib} , and equation (24) can be used for formulating the variational principle for torsional oscillations.

Let us also present the expression for the viscous dissipation rate of the torsional vibration energy, \dot{E}_{vib} , for a distant observer (where dot means differentiation over the Schwarzschild time). It is easily derived using the formalism of Schumaker & Thorne (1983),

$$\dot{E}_{\text{vib}} = \frac{\pi \ell(\ell+1)}{2\ell+1} \omega^2 \int_{r_1}^{r_2} dr \eta r^2 e^{-\Phi-\Lambda} |Y'|^2, \quad (27)$$

where η is the shear viscosity in a neutron star crust (Chugunov & Yakovlev 2005; Shternin 2008). We naturally assume that the dissipation time is much slower than vibration period.

4 PROPERTIES OF TORSIONAL OSCILLATIONS

4.1 Neutron star model

For an example, we have chosen a typical model of a neutron star with $M = 1.4 M_\odot$ and nucleon core. The equation of state is based on the results obtained by Akmal et al. (1998). It was suggested by Gusakov et al. (2005) (and called APR III) using a numerical parameterization of Heiselberg & Hjorth-Jensen (1999, 2000). The stellar radius is $R = 12.27$ km. The neutron drip density $\rho_{\text{drip}} = 4.3 \times 10^{11} \text{ g cm}^{-3}$ is reached at $r_{\text{drip}} = 11.82$ km and $m_{\text{drip}} = 1.3998 M_\odot$. The crust-core interface is placed at $\rho_{\text{cc}} = 1.45 \times 10^{14} \text{ g cm}^{-3}$ (with $r_{\text{cc}} = 10.09$ km and $m_{\text{cc}} = 1.364 M_\odot$). The shear modulus μ in the cold catalyzed crust is calculated from equation (14) using the smooth composition model of spherical nuclei (Haensel et al. 2007). Fig. 1 shows the dependence of μ on ρ (the left-hand vertical axis), as well as the dependence of the local shear-wave velocity v_s on ρ [equation (22), the right-hand axis]. Note that although the smooth composition model averages density variations of μ (produced by variations of nuclear parameters with depth), it formally gives a small jump of μ at the neutron drip point. On the other hand, the problem of accurate calculation of elastic moduli in the deep crust is far from being solved (Haensel et al. 2007) and the exact $\mu(\rho)$ dependence is actually not known. For that reason, we have

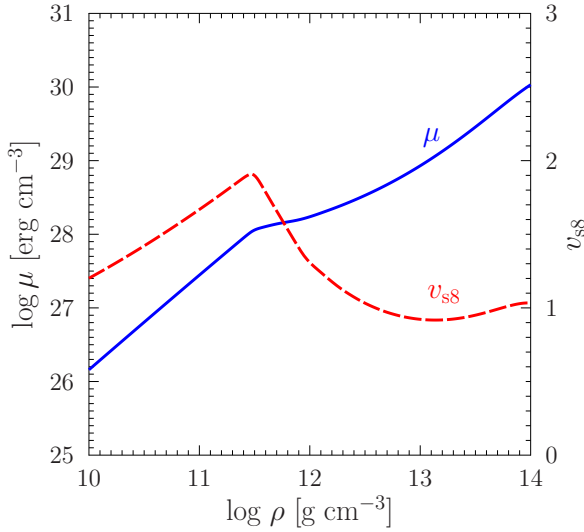


Figure 1. The shear modulus μ (the left-hand vertical axis) and the local shear velocity v_s (in units of 10^8 cm s^{-1} , the right-hand vertical axis) as a function of density in the neutron star crust.

smoothed out artificially the $\mu(\rho)$ jump at the neutron drip point; we will comment on theoretical uncertainties of $\mu(\rho)$ below. In any case Fig. 1 demonstrates different behavior of μ and v_s in the outer and inner crust (separated by the density ρ_{drip}).

4.2 Eigenfrequencies and eigenmodes

Let us analyze torsional oscillation modes (ℓ, n) described by equation (21). The cyclic oscillation frequencies will be denoted as $\nu_{\ell n} = \omega_{\ell n}/(2\pi)$. Equation (21) is easily solved numerically. A solution can be specified by $Y(r_2) = Y_0$ at the outer boundary of the crystalline shell. Any solution gives an eigenfrequency ν as well as radial functions $Y(r)$ and $Y'(r)$. The first function determines horizontal shifts of crystalline matter elements (20), while the second function specifies the only one non-trivial strain tensor element of the problem, $u_{r\phi}$. In a local reference frame we have

$$u_{r\phi} = \frac{rY'(r)}{2\exp\Lambda(r)} b(\theta). \quad (28)$$

It is convenient to characterize $u_{r\phi}$ by the radial strain function defined as

$$\xi(r) \equiv \frac{rY'(r)}{2Y_0 \exp\Lambda(r)}. \quad (29)$$

It is independent of the normalization constant Y_0 and shows how strained the crystal is in a local matter element.

Equation (28) allows us to write down the only one non-trivial elastic stress tensor component of oscillating crystal,

$$\sigma_{r\phi} = \frac{\mu r Y'(r)}{\exp\Lambda(r)} b(\theta), \quad (30)$$

and formulate the local crystal breaking condition. The breaking occurs if $|\sigma_{r\phi}|$ exceeds the breaking stress σ_{max} . Comparing equations (15) and (14) we have $\sigma_{\text{max}} = \alpha_* \mu$,

Table 3. Some torsional oscillation parameters for a $1.4 M_\odot$ neutron star (Y_0 is expressed in radians); see the text for details

ℓ, n	ν [Hz]	E_{vib} [erg]	$ \xi_* ^{(a)}$	$Y_{0*}^{(b)}$	$E_{\text{vib}}^{*(c)}$ [erg]
2, 0	22.77	$1.64 \times 10^{48} Y_0^2$	0.01	$\ll 1$	$\ll 2 \times 10^{48}$
3, 0	36.01	$5.88 \times 10^{48} Y_0^2$	0.03	$\ll 1$	$\ll 6 \times 10^{48}$
2, 1	631.1	$5.30 \times 10^{49} Y_0^2$	9.7	0.006	2×10^{45}
3, 1	631.6	$7.60 \times 10^{49} Y_0^2$	9.7	0.004	1.3×10^{45}
2, 2	1031.3	$1.66 \times 10^{49} Y_0^2$	10	0.006	5×10^{44}
3, 2	1031.6	$2.38 \times 10^{49} Y_0^2$	10	0.004	4×10^{44}

^{a)} Breaking value of radial strain function

^{b)} Breaking or limiting angular vibration amplitude

^{c)} Breaking or limiting vibrational energy

where $\alpha_* \approx 0.02/0.1194 \approx 0.17$ is a constant provided by the theory of deformed Coulomb crystals (Section 2). The breaking occurs in a point r_* at an angle θ_* if the pulsation amplitude Y_0 is sufficiently large,

$$|Y_{0*}| \geq \frac{\alpha_*}{2b(\theta_*)|\xi(r_*)|}. \quad (31)$$

Here r_* refers to the maximum of $|\xi(r)|$, and θ_* to the maximum b_{max} of $|b(\theta)|$. For $\ell = 2$ we have $\theta_* = \pi/4$ and $b_{\text{max}} = 3/2$, while for $\ell = 3$ we obtain $\sin^2 \theta_* = 4/15$ and $b_{\text{max}} = 8/\sqrt{15} \approx 2.066$.

The properties of fundamental torsional modes (without radial nodes, $n = 0$) and ordinary modes (with radial nodes, $n > 0$) are drastically different (e.g., Schumaker & Thorne 1983) and will be described separately. In Table 3 we present numerically calculated frequencies ν and vibration energies E_{vib} for two fundamental modes ($\ell = 2$ and 3 ; $n = 0$) and four ordinary ones ($\ell = 2$ and 3 ; $n = 1$ and 2). The three last columns in Table 3 are concerned with crystal breaking as detailed in the next sections.

4.3 Fundamental torsional oscillations

These oscillations possess remarkable properties associated with the fact that the elastic shear modulus in a neutron star crust is much smaller than the compressional modulus (the latter determines hydrostatic structure of the crust). In the absence of radial nodes, the vibrating crystal remains strongly understrained (non-deformed), with $|\xi(r)| \ll 1$ in the entire crystalline shell. This means that the crystal is almost fully relaxed, with

$$Y(r) \approx Y_0 \quad (32)$$

anywhere at $r_1 \leq r \leq r_2$.

For instance, Fig. 2 shows the radial dependence of $Y(r)$ in the crust of the $1.4 M_\odot$ star (Section 4.1) for the simplest torsional oscillation mode with $\ell = 2$ and $n = 0$. Instead of the radial variable r we use the density variable ρ . The outer crystalline boundary is placed at $\rho = 10^{10} \text{ g cm}^{-3}$ (about 165 m under the surface) and the highest density corresponds to the crust-core interface. We will show that shifting the outer boundary to the surface or inside of the star does not affect the results. The solid line shows (the left-hand vertical axis) the radial strain function ξ defined by equation (29). We see that the values of ξ are indeed small, $|\xi(\rho)| \lesssim 0.01$, so that the crystal stays nearly non-deformed.

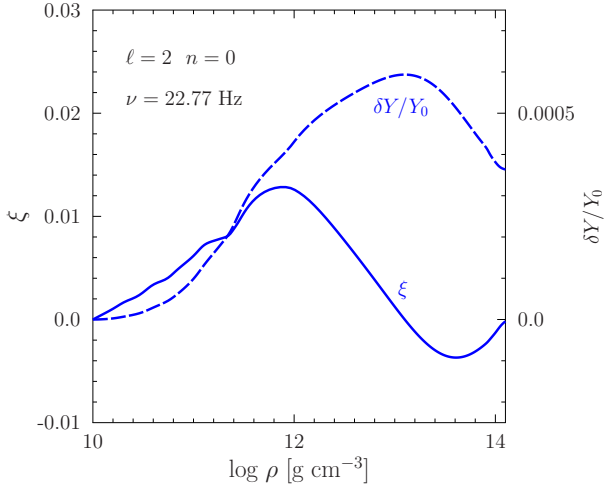


Figure 2. Radial eigenfunctions versus density ρ in the neutron star crust for the mode with $\ell = 2$ and $n = 0$ at $\nu = 22.77$ Hz. The solid line is the radial strain function (29) that is plotted along the left-hand vertical axis. The dashed line demonstrates very weak relative deviations $\delta Y/Y_0$ of $Y(\rho)$ from Y_0 [plotted along the right-hand vertical axis, with $\delta Y = Y(\rho) - Y_0$].

As a result, the approximation (32) is almost perfect. Relative deviations of $Y(\rho)$ from Y_0 are shown on the same Fig. 2 by the dashed line along the right-hand axis. They do not exceed 0.0006.

Note some wiggles of the $\xi(\rho)$ curve near the neutron drip density (Fig. 2). They result from our artificial smoothing of the $\mu(\rho)$ dependence described in Section 4.1. Making more accurate smoothing, we could remove the wiggles. We have left them as a reminder that the reality is usually more complicated than artificially smoothed theoretical curves. The problem of constructing a realistic $\mu(\rho)$ dependence is complicated. On general grounds, one can expect that this dependence is not smooth, especially at those densities, where one preferable nucleus type is replaced by another (e.g., Haensel et al. 2007). This would lead to wiggling of $\xi(\rho)$ [and, to a less extent, of $Y(\rho)$] curves, which may affect torsional oscillations (especially with high n and ℓ).

Having $\xi(r)$ from Fig. 2, we can check the crystal breaking condition (31) for the ($\ell = 2$, $n = 0$) mode. The breaking point would be at $\theta_* = \pi/4$ and $\rho_* \approx 10^{12}$ g cm $^{-3}$. However, since $|\xi(\rho)| \ll 1$, the breaking would require large oscillation amplitudes, $Y_0 \gg 1$, which are beyond the linear oscillation theory. Accordingly, the fundamental torsional oscillations do not break in the linear regime (at $|Y| \ll 1$).

This conclusion holds for all fundamental oscillations which keep the crystal almost relaxed. For instance, Fig. 3 shows the same functions $\xi(\rho)$ and $\delta Y(\rho)/Y_0$ for the next fundamental mode with $\ell = 3$ and $n = 0$. The results are similar although the approximation of almost full relaxation becomes worse with increasing ℓ (the values of $|\xi|$ are getting higher).

The same approximation greatly simplifies calculations of the eigenfrequencies. Indeed, in this case we can use equation (24), neglect the terms containing Y' in equations (26)

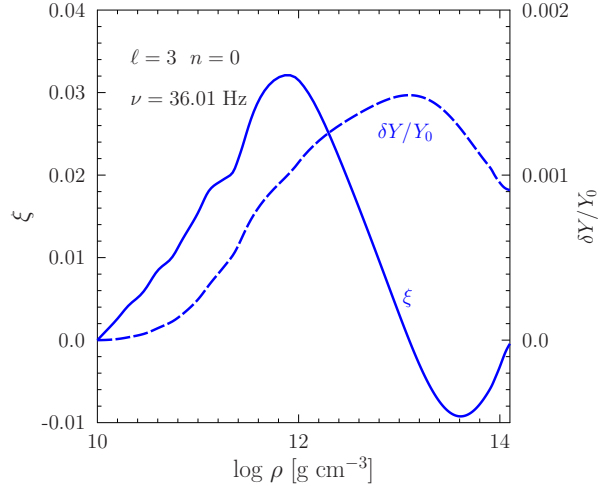


Figure 3. The same as in Fig. 2 but for the mode with $\ell = 3$ and $n = 0$ at $\nu = 36.01$ Hz.

and (25) and set $Y = Y_0$ there. Then we obtain

$$\omega_{\ell 0}^2 = \frac{1}{4} \omega_{20}^2 (\ell + 2)(\ell - 1), \quad \omega_{20}^2 = \frac{8E_\mu}{3I_{\text{cr}}}, \quad (33)$$

$$I_{\text{cr}} = \frac{8\pi}{3} \int_{r_1}^{r_2} dr r^4 (\rho + P/c^2) \exp(\Lambda - \Phi), \quad (34)$$

$$E_\mu = 4\pi \int_{r_1}^{r_2} dr r^2 \mu \exp(\Phi + \Lambda). \quad (35)$$

This is an explicit analytic expression for the pulsation frequencies $\omega_{\ell 0}$ in terms of two simple one-dimensional integrals, I_{cr} and E_μ , which are easily computed once a neutron star model and crustal microphysics are known. If we set $\exp \Phi(r) = 1$ under the integrals (as if we ignore gravitational time delay of signals for a distant observer), we would immediately identify I_{cr} as the moment of inertia of the crust and E_μ as the shear modulus integrated over the crust (which is close to the total electrostatic Coulomb energy of the crust). The factor $\exp \Phi(r)$ under the integrals is needed to express ω for a distant observer. To the best of our knowledge, this explicit representation of torsional fundamental pulsation frequencies has not been known in the literature.

In our case, $E_\mu = 6.85 \times 10^{47}$ erg and $I_{\text{cr}} = 8.91 \times 10^{43}$ g cm 2 . We have checked that equation (33), indeed, accurately reproduces the frequencies $\nu_{\ell 0}$ of fundamental modes derived by solving the basic differential equation (21).

According to equation (33), the spectrum of fundamental modes is expressed through the lowest frequency ω_{20} and multipolarity ℓ and behaves as $\omega_{\ell 0} \propto \sqrt{(\ell - 1)(\ell + 2)}$, which gives, for instance, $\omega_{30}/\omega_{20} = \sqrt{2.5} = 1.581$. At large ℓ the neighboring frequencies become equidistant. However, some publications predict, from qualitative considerations, another scaling $\omega_{\ell 0} \propto \sqrt{\ell(\ell + 1)}$ [e.g. equation (3a) in Schumaker & Thorne 1983, or equation (3) in Sotani 2016]; it gives $\omega_{30}/\omega_{20} = \sqrt{2} = 1.414$. We see that the exact form is somewhat different from the approximate one.

We should stress that the correctness of the scaling $\omega_{\ell 0} \propto \sqrt{(\ell - 1)(\ell + 2)}$ has been discussed in the literature, although it has not been written in an explicit form (33).

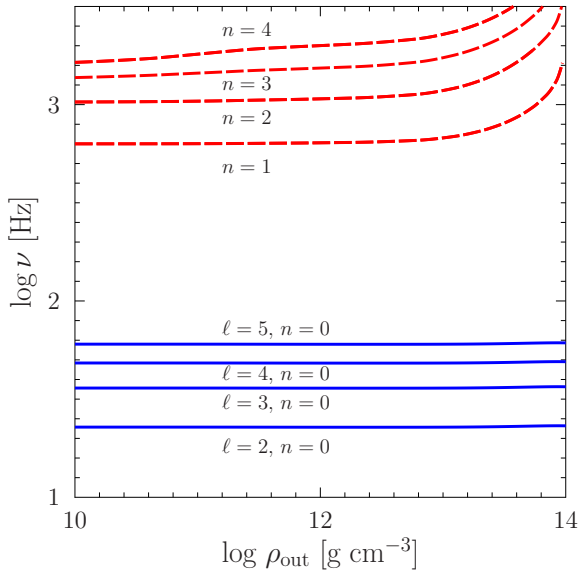


Figure 4. Spectrum of torsional oscillations localized in an artificial crust, where the matter is crystallized only within the shell located starting from some outer density ρ_{out} to the crust-core interface, as a function of ρ_{out} . Four lower solid lines refer to fundamental modes with $\ell = 2, 3, 4, 5$ (from bottom to top). The dashed lines refer to ordinary modes with $n = 1, 2, 3, 4$. Each dashed line encloses a number of modes with $\ell = 2, 3, 4$, whose frequencies are non-distinguishable in the logarithmic scale.

In particular, [Samuelsson & Andersson \(2007\)](#) present very convincing arguments (based on many numerical calculations) that the ratio $\omega_{30}/\omega_{20} = \sqrt{2.5}$ is true. [Gabler et al. \(2016\)](#) in their table 2 present the frequencies $\omega_{\ell 0}$ with ℓ from 2 to 6, which agree with the correct scaling (except for $\ell = 6$, where the frequency contains the typo and should be 83.8 Hz). However, [Sotani \(2016\)](#) prefer to use the approximate scaling to fit the fundamental oscillation frequencies.

The approximation of almost relaxed crystal allows us to use equation (23) and obtain the energy of any fundamental mode in analytic form,

$$E_{\text{vib}}^{\ell 0} = \frac{(\ell - 1)\ell(\ell + 1)(\ell + 2)}{2(2\ell + 1)} E_{\mu} Y_0^2. \quad (36)$$

This formula seems original as well. The vibration energy is determined by the Coulomb energy of the crust and by the angular vibration amplitude Y_0 (expressed in radians). For instance, for the mode with $\ell = 2$ and $n = 0$ we have $E_{\text{vib}}^{20} \approx 1.64 \times 10^{48} Y_0^2$ erg, meaning that the energy can be quite substantial. Since the applicability of this expression is limited by the linear vibration regime ($Y_0 \ll 1$), we conclude that the expression is valid as long as $E_{\text{vib}}^{20} \ll 2 \times 10^{48}$ erg.

Another remarkable property of torsional vibrations is shown in Fig. 4. This figure exhibits the spectrum of oscillations with $\ell = 2, 3$ and 4 and $n = 0, \dots, 4$. The frequencies are computed from the differential equation (21) by artificially assuming that the crystallized shell occupies some fraction of the crust, starting from an arbitrary density ρ_{out} and ending at the crust-core interface (as if the layer at $\rho < \rho_{\text{out}}$

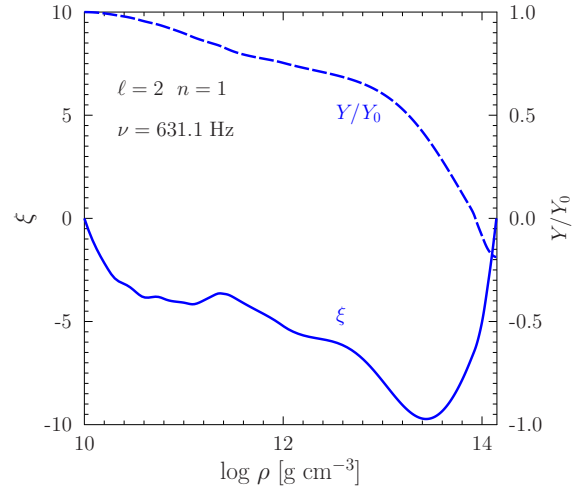


Figure 5. Radial eigenfunctions versus density ρ in the neutron star crust for the $(\ell = 2, n = 1)$ mode with the frequency $\nu = 631.06$ Hz. The solid line is the radial strain function (29) that is plotted along the left-hand vertical axis. The dashed line demonstrates variations of $Y(\rho)/Y_0$ (the right-hand vertical axis).

is melted). The frequencies are plotted in logarithmic scale versus $\log \rho_{\text{out}}$.

Four lowest solid lines refer to the family of fundamental modes ($\ell = 2, 3, 4, 5$ with $n = 0$) which are approximately equidistant in the linear scale. These frequencies are well described by equation (33). Their most interesting feature is that they are almost insensitive to ρ_{out} : an artificial melting of any outer layer of the crust has almost no effect on the spectrum of fundamental modes. This feature seems to be closely related to the almost relaxed state of crystals in fundamental oscillations.

The dashed lines on Fig. 4 correspond to ordinary torsion modes with $n = 1, \dots, 4$ (from bottom to top). Each dashed curve shows actually a family of different modes with $\ell = 2, 3$ and 4, but the ‘fine splitting’ of the curves with different ℓ is so small that it is invisible in the logarithmic format. These modes will be analyzed below.

4.4 Ordinary torsional oscillations

Now let us turn to torsional oscillations with radial nodes ($n > 0$). They are less remarkable. The main difference from the fundamental modes is that now crystalline matter is rather strained and stressed. The analytic expressions for the pulsation frequencies (33) and energies (36) become inapplicable; one should calculate these quantities from more complicated equations (21) and (23).

For example, Fig. 5 shows the radial strain function $\xi(\rho)$ (the left-hand vertical axis) and the function $Y(\rho)/Y_0$ (the right-hand vertical axis) for the simplest ($\ell = 2, n = 1$) mode. One can observe single radial node of $Y(\rho)$ in the inner crust at $\rho = 8.6 \times 10^{13}$ g cm $^{-3}$. A comparison with Fig. 2 (for $\ell = 2, n = 0$) shows that now the radial strain function $|\xi(\rho)|$ is much larger and reaches the values $|\xi| \sim 10$. The vibrating crust becomes dynamically deformed, which increases pulsation frequencies ($\nu_{21} = 631.06$ Hz versus

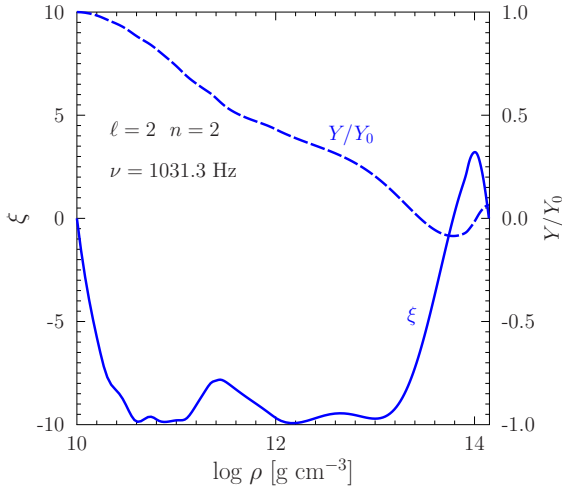


Figure 6. Same as in Fig. 5 but for the $(\ell = 2, n = 2)$ mode with $\nu = 1031.3$ Hz.

$\nu_{20} = 22.77$ Hz; see Table 3). For the same angular pulsation amplitude Y_0 , the pulsation energy E_{vib}^{21} is about 30 times higher than E_{vib}^{20} .

Since the $(\ell = 2, n = 1)$ mode is strained, it can break in the linear pulsation regime. The breaking occurs (Fig. 5) in the inner crust at $\rho_* \approx 2.8 \times 10^{13} \text{ g cm}^{-3}$, where $|\xi(\rho)|$ reaches maximum, $|\xi_*| \approx 9.7$, provided the pulsation amplitude reaches the breaking value $|Y_{0*}| \approx 0.0058$ given by equation (31). This crystal breaking limits the maximum vibrational energy to $E_{\text{vib}}^* \approx 6 \times 10^{47}$ erg in the linear pulsation regime.

Recall that the pulsation frequencies $\nu_{\ell k}$ of modes with given $n > 0$ slightly increase with ℓ (Table 3, Fig. 4), demonstrating the ‘fine splitting’ structure (which was pointed out long ago; e.g., Hansen & Cioffi 1980). The deformation profiles $Y(\rho)$ and $\xi(\rho)$ for such modes, as well as breaking densities ρ_* , are also slightly dependent of ℓ . Our estimates of breaking vibration amplitudes $|Y_{0*}|$ and vibrational energies E_{vib}^* for some modes are presented in Table 3.

Fig. 6 shows $Y(\rho)$ and $\xi(\rho)$ for the mode with $\ell = 2$ and $n = 2$. This mode is more complicated, with the two nodes of $Y(\rho)$ at $\rho \approx 2.8 \times 10^{13}$ and $1.03 \times 10^{14} \text{ g cm}^{-3}$ near the crust-core interface. The crystal is more stressed there, which rises the oscillation frequency to $\nu = 1.0313$ kHz. Such oscillations of $Y(\rho)$ are becoming sensitive to small uncertainties (wiggles) of the shear modulus $\mu(\rho)$ (discussed above); their breaking can occur in the outer crust. Therefore, theoretical construction of high-frequency torsional oscillations can be dependent on largely unknown details of the shear modulus behavior.

Now we return to the spectra of oscillation frequencies in a theoretical experiment of artificial ‘melting’ the outer layer of the crust (from the surface to ρ_{out} ; Fig. 4). In contrast to the fundamental modes, the vibration frequencies of ordinary modes (dashed curves) may considerably depend on ρ_{out} . Nevertheless, this dependence is most pronounced at sufficiently high ρ_{out} , when the ‘melting’ reaches the inner crust. Shallower melting has almost no effect on $\nu_{\ell n}$. It looks as if the outer crust does not affect the torsional oscillation

frequencies at all, so that theorists can remove it while calculating $\nu_{\ell n}$. Its only duty is to allow the matter to vibrate near the surface for making the vibrations observable.

This effect has a simple explanation. The oscillations are definitely controlled in the inner crust, where crystalline matter can be strongly stressed. In contrast, oscillations of the outer crystalline layers remain rather relaxed and do not affect $\nu_{\ell n}$. Accordingly, the oscillation frequencies are almost insensitive to the physics of the outer crust (cold-catalyzed or accreted matter, mono-crystal or isotropic solid, one ion component or mixture of different ions, exact position of outermost melted layers and type of outer boundary condition).

5 DISCUSSION AND CONCLUSIONS

We have studied deformed crystalline matter in neutron star crust. Firstly, in Section 2 we have performed semi-analytic calculations of the breaking stress of Coulomb mono-crystals of atomic nuclei under shear deformations of two types, (8) and (12), taking into account the electron plasma screening of Coulomb forces between the nuclei. We have fitted the results by the analytic expression (10). We have also analysed the breaking stress of Coulomb crystals in the model of isotropic solid, which is needed for applications.

Secondly, we have presented some new results on torsional oscillations of spherically symmetric and non-magnetic neutron star crust. In particular, we have derived exact analytic expressions (33) and (36) for frequencies and energies of fundamental torsional oscillations, analyzed the same quantities for ordinary torsional oscillations, and pointed out a specific independence of the torsional vibrations of physical conditions in the outer crust. In addition, we have formulated the conditions for breaking the torsional oscillations. The torsional pulsation spectra have been extensively studied before, but pulsation energies, distribution of deformations and stresses over oscillating crust, and the breaking conditions have been given little attention.

The spectra of torsional oscillations in spherical non-magnetic stars have been analyzed in many publications (e.g., Andersson et al. 2009; Sotani et al. 2012, 2013a,b; Sotani 2016, and references therein). The authors have used different modern equations of state of neutron star matter and wide ranges of neutron star masses with the aim to explore the sensitivity of oscillation spectra on the equation of state and nuclear physics of the matter near the crust-core interface (the density dependence of the symmetry energy, possible presence of nuclear pasta phases, superfluidity of neutrons). We have intentionally chosen one equation of state and one neutron star mass because the effects of different equations of states and masses have already been explored.

So far, the theory of torsional oscillations has been employed to interpret spectra of QPOs observed in X-ray tails of flares of three SGRs. SGRs belong to a class of magnetars; their flaring activity is regulated by very strong magnetic fields, $B \sim 10^{15} \text{ G}$ (see, e.g., Mereghetti et al. 2015; Kaspi & Beloborodov 2017, for a recent review). These QPOs were detected in the hyperflare of SGR 1806–20 (in 2004), in the giant flare SGR 1900+14 (1998), and in sequences of numerous less energetic recur-

rent bursts of SGR 1806–20 (1996) and SGR J1550–5418 (2009) (e.g., [Israel et al. 2005](#); [Watts & Strohmayer 2006](#); [Hambaryan et al. 2011](#); [Huppenkothen et al. 2014b,a](#), and references therein). For example, the frequencies of QPOs discovered in the afterglow of the hyperflare of SGR 1806–20 are 18, 26, 30, 92, 150, 625, 1840 Hz and (with somewhat less confidence) 17, 21, 36, 59, 116 Hz. The QPO frequencies detected in other events range from 28 to 260 Hz.

All these QPOs can (in principle) be explained by torsional oscillations of spherical non-magnetic neutron stars. However, the current state of the art in neutron star physics strongly suggests to include important effects of high magnetic fields, superfluidity of nucleons and other effects of nuclear interactions (like entrainment) in the stellar core. There have been many investigations of global low-frequency oscillations of magnetized superfluid neutron stars (e.g., [Levin 2006, 2007](#); [Glampedakis et al. 2006](#); [Sotani et al. 2007](#); [Cerdá-Durán et al. 2009](#); [Colaiuda et al. 2009](#); [Colaiuda & Kokkotas 2011, 2012](#); [van Hoven & Levin 2011, 2012](#); [Gabler et al. 2011, 2012, 2013b,a, 2016, 2018](#); [Passamonti & Lander 2014](#); [Link & van Eysden 2016](#)). A comprehensive discussion of the current state of the affair can be found in [Gabler et al. \(2016, 2018\)](#). The two major ingredients of the theory are torsional crustal oscillations (affected by crustal magnetic fields) and continuum of Alfvén shear waves in the core. Interaction of these waves leads to the appearance of discrete spectrum of magneto-elastic oscillations. The spectrum essentially depends on the magnetic field strength and geometry and on superfluid properties of neutron star matter. These oscillations can also be coupled with MHD oscillations in magnetospheres of magnetars (e.g., [Link & van Eysden 2016](#)).

The theory enables one to interpret QPOs in SGRs, but possible interpretations seem still not unambiguous because of vast diversity of theoretical models and associated degeneracy in the parameter space. Some theoretical problems have not been considered yet, for instance, possible effects of hyperons in neutron star cores and many sophisticated relativistic MHD effects (e.g. [Dommes et al. 2020](#)). This motivates further studies of magneto-elastic oscillations.

Our results can be useful for describing these oscillations in the crust. Note that we have not touched the problem of oscillation excitation and damping, as well as the transformation of the oscillations into observable QPOs. Torsional oscillations in idealized spherical non-magnetic stars could live for a long time. Their decay times due to gravitational radiation were estimated ([Schumaker & Thorne 1983](#)) to be about 10^4 years, and damping due to shear viscosity calculated from equation (27) would be even much longer. In contrast, QPOs in SGR flares loose coherence in a fraction of second, which suggests QPOs cannot be just ordinary torsional crustal oscillations. There are many channels of fast damping of oscillations in magnetized stars discussed in the references cited above (e.g., [Gabler et al. 2011](#)). Also, there could be different mechanisms for excitation of the magneto-elastic oscillations in flaring SGRs (e.g. [Beloborodov & Li 2016](#)).

Let us stress that magneto-elastic oscillations in SGRs can be very different from classical torsional oscillations in non-magnetic crust. Superflares of SGRs are accompanied by enormous energy release (e.g. [Beloborodov & Li 2016](#)), making the crust hot and melting some regions, especially

outer layers, where the melting temperature is sufficiently low. According to our results (Fig. 4), such a melting does not affect the oscillation frequencies, which supports the idea that QPOs are connected with magneto-elastic oscillations. However, an additional study is required to show that our results remain valid under SGR conditions.

Our results can also be useful to simulate other processes involving deformed crystals in neutron stars like evolution of the crustal magnetic fields (e.g., [Beloborodov & Levin 2014](#); [Lander 2016](#); [Li et al. 2016](#)) and pulsar glitches (e.g., [Piekarewicz et al. 2014](#)).

ACKNOWLEDGMENTS

We are grateful to D. Baiko for providing us the data on deformed Coulomb crystals and to the anonymous referee for pointing out that our results may support the connection of QPOs in flaring SGRs with magneto-elastic oscillations. The work was supported by the Russian Science Foundation (grant 19-12-00133).

DATA AVAILABILITY

The data underlying this article will be shared on reasonable request to the authors.

References

- Akmal A., Pandharipande V. R., Ravenhall D. G., 1998, *Phys. Rev. C*, 58, 1804
- Andersson N., Glampedakis K., Samuelsson L., 2009, *MNRAS*, 396, 894
- Baiko D. A., 2002, *Phys. Rev. E*, 66, 056405
- Baiko D. A., Chugunov A. I., 2018, *MNRAS*, 480, 5511
- Baiko D. A., Kozhberov A. A., 2017, *MNRAS*, 470, 517
- Beloborodov A. M., Levin Y., 2014, *ApJ*, 794, L24
- Beloborodov A. M., Li X., 2016, *Astrophys. J.*, 833, 261
- Cerdá-Durán P., Stergioulas N., Font J. A., 2009, *MNRAS*, 397, 1607
- Chamel N., Fantina A. F., 2016, *Phys. Rev. C*, 94, 065802
- Chamel N., Haensel P., 2008, *Living Reviews in Relativity*, 11, 10
- Chugunov A. I., Horowitz C. J., 2010, *MNRAS*, 407, L54
- Chugunov A. I., Horowitz C. J., 2012, *Contributions to Plasma Physics*, 52, 122
- Chugunov A. I., Yakovlev D. G., 2005, *Astronomy Reports*, 49, 724
- Colaiuda A., Kokkotas K. D., 2011, *MNRAS*, 414, 3014
- Colaiuda A., Kokkotas K. D., 2012, *MNRAS*, 423, 811
- Colaiuda A., Beyer H., Kokkotas K. D., 2009, *MNRAS*, 396, 1441
- Dommes V. A., Gusakov M. E., Shternin P. S., 2020, *Phys. Rev. D*, 101, 103020
- Fattoyev F. J., Horowitz C. J., Lu H., 2018, arXiv e-prints, p. arXiv:1804.04952
- Gabler M., Cerdá-Durán P., Font J. A., Müller E., Stergioulas N., 2011, *MNRAS*, 410, L37
- Gabler M., Cerdá-Durán P., Stergioulas N., Font J. A., Müller E., 2012, *MNRAS*, 421, 2054
- Gabler M., Cerdá-Durán P., Stergioulas N., Font J. A., Müller E., 2013a, *Phys. Rev. Lett.*, 111, 211102
- Gabler M., Cerdá-Durán P., Font J. A., Müller E., Stergioulas N., 2013b, *MNRAS*, 430, 1811
- Gabler M., Cerdá-Durán P., Stergioulas N., Font J. A., Müller E., 2016, *MNRAS*, 460, 4242

- Gabler M., Cerdá-Durán P., Stergioulas N., Font J. A., Müller E., 2018, *MNRAS*, 476, 4199
- Glampedakis K., Samuelsson L., Andersson N., 2006, *MNRAS*, 371, L74
- Gusakov M. E., Kaminker A. D., Yakovlev D. G., Gnedin O. Y., 2005, *MNRAS*, 363, 555
- Haensel P., Potekhin A. Y., Yakovlev D. G., 2007, Neutron Stars. 1. Equation of State and Structure. Springer, New York
- Hamaguchi S., Farouki R. T., 1994, *J. Chem. Phys.*, 101, 9876
- Hambaryan V., Neuhäuser R., Kokkotas K. D., 2011, *A&A*, 528, A45
- Hansen C. J., Cioffi D. F., 1980, *ApJ*, 238, 740
- Heiselberg H., Hjorth-Jensen M., 1999, *ApJ*, 525, L45
- Heiselberg H., Hjorth-Jensen M., 2000, *Phys. Rep.*, 328, 237
- Hoffman K., Heyl J., 2012, *MNRAS*, 426, 2404
- Horowitz C. J., Hugto J., 2008, arXiv e-prints, p. arXiv:0812.2650
- Horowitz C. J., Kadau K., 2009, *Phys. Rev. Lett.*, 102, 191102
- Hugto J., 2012, in Journal of Physics Conference Series. p. 012005, doi:10.1088/1742-6596/342/1/012005
- Huppenkothen D., et al., 2014a, *ApJ*, 787, 128
- Huppenkothen D., Heil L. M., Watts A. L., Göğüş E., 2014b, *ApJ*, 795, 114
- Israel G. L., et al., 2005, *ApJ*, 628, L53
- Kaspi V. M., Beloborodov A. M., 2017, Annual Rev. Astron. Astrophys., 55, 261
- Kozhberov A., 2018, PhD thesis, Ioffe Institute, St Petersburg
- Lander S. K., 2016, *ApJ*, 824, L21
- Levin Y., 2006, *MNRAS*, 368, L35
- Levin Y., 2007, *MNRAS*, 377, 159
- Li X., Levin Y., Beloborodov A. M., 2016, *ApJ*, 833, 189
- Link B., van Eysden C. A., 2016, *ApJ*, 823, L1
- Mereghetti S., Pons J. A., Melatos A., 2015, Space Sci. Rev., 191, 315
- Ogata S., Ichimaru S., 1990, *Phys. Rev. A*, 42, 4867
- Owen B. J., 2005, *Phys. Rev. Lett.*, 95, 211101
- Passamonti A., Lander S. K., 2014, *MNRAS*, 438, 156
- Piekarewicz J., Fattoyev F. J., Horowitz C. J., 2014, *Phys. Rev. C*, 90, 015803
- Robbins M. O., Kremer K., Grest G. S., 1988, *J. Chem. Phys.*, 88, 3286
- Samuelsson L., Andersson N., 2007, *MNRAS*, 374, 256
- Schumaker B. L., Thorne K. S., 1983, *MNRAS*, 203, 457
- Shapiro S. L., Teukolsky S. A., 1983, Black holes, white dwarfs, and neutron stars: The physics of compact objects. Wiley-Interscience, New York
- Shternin P. S., 2008, *Journal of Physics A Mathematical General*, 41, 205501
- Sotani H., 2016, *Phys. Rev. D*, 93, 044059
- Sotani H., Kokkotas K. D., Stergioulas N., 2007, *MNRAS*, 375, 261
- Sotani H., Nakazato K., Iida K., Oyamatsu K., 2012, *Phys. Rev. Lett.*, 108, 201101
- Sotani H., Nakazato K., Iida K., Oyamatsu K., 2013a, *MNRAS*, 428, L21
- Sotani H., Nakazato K., Iida K., Oyamatsu K., 2013b, *MNRAS*, 434, 2060
- Strohmayer T., Ogata S., Iyetomi H., Ichimaru S., van Horn H. M., 1991, *ApJ*, 375, 679
- Vaulina O. S., Koss X. G., Khrustalyov Y. V., Petrov O. F., Fortov V. E., 2010, *Phys. Rev. E*, 82, 056411
- Watts A. L., Strohmayer T. E., 2006, *ApJ*, 637, L117
- van Hoven M., Levin Y., 2011, *MNRAS*, 410, 1036
- van Hoven M., Levin Y., 2012, *MNRAS*, 420, 3035